Weight Prediction of the Lifting System for an Unconventional Aircraft Configuration

G.L. Ghiringhelli[a], A. Frediani[b], M. Terraneo[c]

[a] Politecnico di Milano
Dipartimento di Scienze e Tecnologie Aerospaziali, Milano, Italy

[b] Università di Pisa
Dipartimento di Ingegneria Industriale, Pisa, Italy

[c] Vicoter
Calolziocorte (LC),Italy

1. Introduction

In the report *A Vision for 2020*, [1], [2] the European Commission set up a list of goals for the aircraft industry to be met by 2020. In the report, the future of aviation is discussed, as well as the challenges laying ahead of its development. Future aviation will need to respond to restrictive imperatives in terms of costs, environmental impact and safety. These challenges are driving goals that are meant to serve as guidelines for future aviation developments.

The future commercial success of the aircraft industry will strongly depend on the improvement of aerodynamic design in terms of drag. In cruise, the drag of a very large transport aircraft is mainly composed of friction and induced drag, accounting for $45 - 48\%$ and $41 - 44\%$ of the total drag respectively. Methods for reducing friction drag, e.g. boundary layer suction and turbulent flow control, are being investigated, but the results are not yet really impressive. In case of a breakthrough in this field, the solution would be applicable to any aircraft configuration. The induced drag mainly depends on the lift distribution over the wing span. Reducing this drag would have significant effects on fuel consumption. The fraction of induced drag becomes more important at low speeds, i.e. during take-off and landing, typically around $80 - 90\%$ ([3]- [6]). The means for reducing induced drag are basically increasing the wing span and improving the lift distribution along the span. A 10% increase in wing span would lead to a 17% reduction in induced drag at constant lift and speed; this would however increase structural weight and, furthermore, this approach, for very large airplanes of the class of an A380, is limited by airport compatibility requirements. On current airliners, the lift distribution is carefully optimized for induced drag through CFD computations: further improvement will thus neither be easily obtained nor quite large. Due to the limitations of conventional designs, new concepts are needed for future aviation [7]- [11] in order to meet the severe requirements imposed by the Vision 2020 report. Several concepts are already being studied and tested. As shown by recent surveys in this field, manufacturers seem to be interested in these new advanced concepts, but with a limited budget to be invested. A huge work has been done on the evaluation of aerodynamic performances

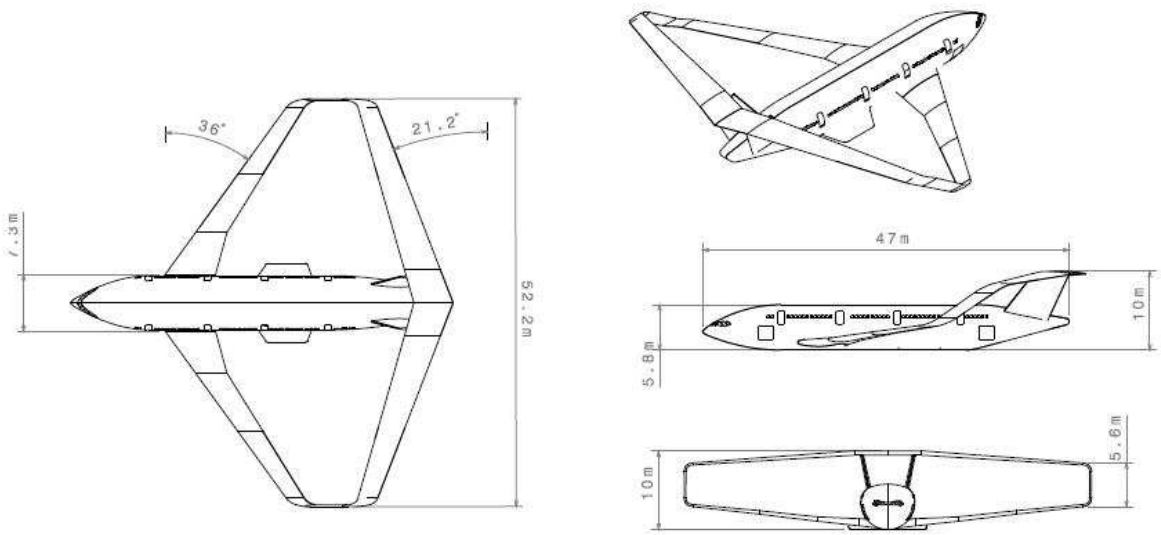

Figure 1. Prandtl Plane 250 configuration

of innovative configurations; e.g. refs [12]- [18] in the case of joined wings aircraft. Tools are needed to reliably predict the weight of such unconventional configurations, as weight is critical in meeting both mission and design requirements; tools are also needed to gain structural insight, essential to anticipate problems related to unconventional configurations. Indeed the accurate weight prediction of wing-box is still matter of inquiries even for traditional aircraft configurations ([19], [20], [21]). Such predictions are fundamentals for multi-disciplinary optimization ([22], [23]) aimed at the preliminary design of an aircraft, especially in case of unconventional or very large aircraft and in the case of composite materials, all situations where semi-empirical formulas are not reliably applicable. This paper is addressed to the assessment of a procedure for the prediction of the structural wing weight specifically implemented to face the case of a box-wings lifting system, namely the PrandtlPlane configuration: this in honor of Ludwig Prandtl that in 1924 found the *Best Wing System*, that is the most efficient lifting system with respect to induced drag.

In theory, this configuration can reduce induced drag up to about 30% with respect to an optimum monoplane configuration [6]. The PrandtlPlane configuration, although proposed in the 90s, still conforms to the *Vision 2020* requirements and has been recently studied in terms of aerodynamic optimization of the general configuration (Ref. [6], [24]) where the benefits of this configuration are widely described. One of the critical areas of research to meet the requirement on aircraft performance is the structural design, in particular of the lifting system. A preliminary study is presented in this paper, referred to a 250-300 passenger civil transport aircraft; its conceptual design (Ref. [6] , [28] and [29]) is in progress at Pisa University (Italy) and the general layout is shown in Fig.1. The fuselage has two decks; the cargo deck holds 38 LD1 containers while the passenger deck is two-isled with 10 passengers abreast for a total of 329 passengers in three classes (270 economy, 49 business ad 16 first). The maximum take-off weight (MTOW) is of 230 tons. This aircraft can be compared, for number of passengers and range, to some conventional liners, namely Airbus$A330-300$, Boeing $B767-300$ and $B777-300$. In this paper, the tool described in Ref. [25] is extended to obtain a more reliable prediction of the lifting system structural weight for such unconventional configuration; the upgrading likely could improve the predictions for conventional ones too. They have been focused during an extensive application of the mass estimation method to the PradtlPlane case and will be discussed in more detail in the following sections. The approach exploits a simplified beam model of the wing box in order to obtain a trial distribution of sectional stiffnesses along the wing span, able to meet both global and local constraints; global constraints, e.g. aileron effectiveness, static aeroelasticity and flutter, are evaluated in terms of global model responses, while local ones, e.g. maximum stress, panel and stiffener instability, are assessed by means of approximated models. The various constraints are activated one at time in order to gather knowledge on the behavior of an unconventional configuration and to be able to appreciate the effect of each of them on the final solution.

2. Structural design of the lifting system

The lifting system is composed of two opposite swept wings, connected at their tips by two vertical wings. They provide the kinematical link between the

wings and transmit internal loads from one wing to the other. The two wings are loaded in a complex way, but the most relevant difference with respect to a conventional configuration lies in the bending moments: due to the overconstrained architecture the null value is far from the wings tips. The rear wing is installed on two fins, that provide lateral control and stability; they also play an important role from a structural standpoint by transferring lift loads generated by the rear wing to the fuselage. Goal of such preliminary design process is just a reliable prediction of the structural weight even for unconventional airplane configurations since the conceptual design phase. In theory this objective should be achieved by using constraints and performances of global kind, while leaving the introduction of local requirements to further investigations, because of lack of information on structural details. This approach however demonstrated to be inefficient, with biased results, so that a further cross section design driven by stiffness requirements was unoptimal. To bypass these problems the set of global constraints has been implemented with local design constraints, even in such preliminary study, by exploiting approximated formulas; the output of the design being represented by the cross section stiffness behavior, this approach leaves the possibility to redefine the local sizing in next design steps without changing the global performances once the cross section stiffness is maintained. Thus the most relevant targets of the structural design of the lifting system are tackled, even in such a preliminary phase; e.g. to provide structural stiffness, to prevent aeroelastic static phenomena, to maintain the aerodynamic efficiency, to generate the necessary structural strength in order to bear loads and to meet local stability requirements. Indeed, the matching of global constraints becomes critical for the PrandtlPlane due to the small dimensions of the wing sections, which reduce the geometric leverages; furthermore the benefits of inertial relief is reduced because of a limited amount of fuel storable in the wings, . The weight estimation exploits a design process of the wing that involves the use of various multidisciplinary optimization activities in order to find the best weight estimate in terms of minimum structural weight attainable while respecting all of the design constraints adopted. [30]- [33] In the present work the interest is mainly focused on two topics: the verification of the potentialities of the method in the case of unconventional configurations and a preliminary discussion of structural solutions for a Prandtlplane aircraft. According to this focus an aluminum alloy wing box has been chosen to study instead a carbon fiber one, also available. In this way a comparison with real, existing aircraft can be performed and the differences found can be blamed to the configuration only. The bias of the contemporary introduction of a new configuration and innovative material is so avoided and the results

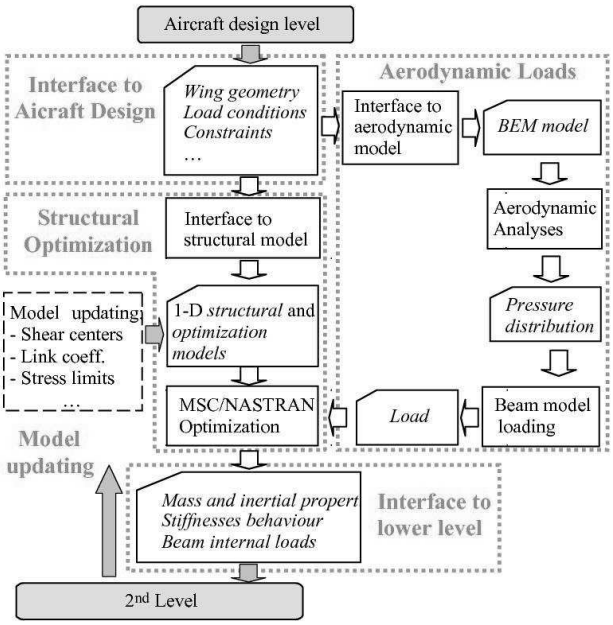

Figure 2. Structural design process

obtained become simply comparable.

3. Weight estimation procedure

This section describes the optimization procedure used in this frame to predict an estimate of the primary structural weight of a wing systems according to different kinds of design constraints. This procedure cannot be discussed in terms of a classical structural optimization, as it is simply devoted to extending the capabilities of simpler approaches for weight estimation (e.g. Ref. [34]) while accounting for requirements on aeroelastic behavior and torsional stiffness and supplying general information on a possible cross section layout, e.g. a preliminary weight budget for skins, webs and stiffeners. The basic idea is to join two problems: the definition of the wing stiffness distributions along wingspan, that grant the matching of global requirements, and the wing box weight prediction, in terms of mass of the structural material needed to give such stiffnesses. Such wing description, in terms of the sectional stiffnesses, represents the starting point for the next design phase in which a more detailed investigation of the box is performed using such stiffnesses as design drivers. On the other hand reliable weight estimations can be exploited in the conceptual design for flight mechanics analyses and compared to different solutions. According to this remarks a global simplified model is used to describe the behavior of the wing: it is a stick model made of simple onedimensional beam elements. This kind of model has been confirmed to be suitable for this kind of purposes (Ref. [42]). A model is needed to link beam cross section stiffness to weight: the predicted mass is assumed to be the

lower amount of structural material suitable to grant the satisfactory global behavior, e.g. the flutter clearance as well as a roll effectiveness. An optimization system is used, exploiting such requirements in terms of design constraints. The present method is mainly suitable to obtain a first weight estimate of the lifting system primary structure for unconventional configuration, such as the joined wing, but it is also applicable when the classical semi-empirical formulae are no longer adequate, e.g. very high WTO aircraft, such as the $A-380$. The next sections describe the models adopted.

3.1. Structural model

The structural model is built exploiting the flexibility of common finite element codes. The layout of the process, with the interactions between the different computer codes, is shown in Fig.2; in this figure the link with a second level design process, suitable for the local design of cross sections, is also sketched: it has been conceived in the frame of a multilevel design optimization of the wingbox, thus an iterative process is envisaged, but it is not exploited in this work.

The process starts with the translation of the basic aircraft design into structural and aerodynamic models; they are automatically generated in term by using a reduced set of geometric data, such as platform, airfoils and twist angles along the span (see Fig.3). The

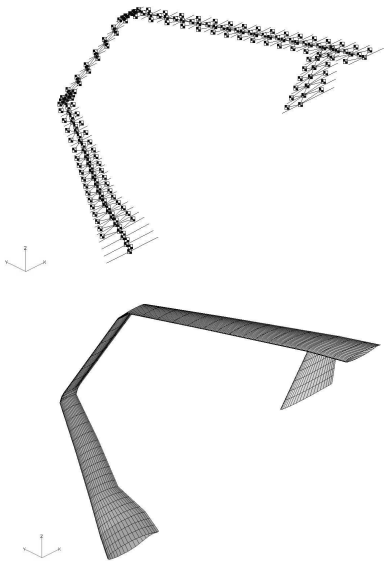

Figure 3. Structural and aerodynamic model of the PP250 (Isometric view)

initial data include nonstructural mass (such as the mass of the leading and trailing edges) as well as fuel mass. The latter is located accounting for the available internal volume. According to choices previously discussed, the material adopted is a typical Aluminum alloy, as suggested in Ref. [34] and related mechanical data are listed in Table 1.

Table 1
Aluminium alloy properties

Description	Value
Density	2800 kg/m3
Young's modulus	70 GPa
Poisson's ratio	0.33
Shear modulus	27 GPa
Admissible yield stress	233 MPa

Standard assumptions are made on the shape of the wing box to determine the front and rear spar positions (20% and 70% of the local wing chord, respectively). According to comments in Ref. [25] the location of the shear centers has been assumed in the middle point of the local wing-box chord) while the rib spacing (0.75m), which is fixed during the optimization, is quite common in jet liner design. Leading edge, trailing edge and rib nonstructural masses are included in the model but they are not subject to optimization. The structural weight of the high lift devices, $7922kg$, has been derived from Ref. [29]. Secondary structures and systems weights are predicted using the same empirical approaches or statistical formulae as for a conventional aircraft [34]- [36] , assuming that their design is only marginally affected by the airframe configuration. Table 2 reports the values of the nonstructural components for a half-wing. The structural model

Table 2
Nonstructural component masses (half wing)

	Fuel mass [kg]	Leading edge mass [kg]	Trailing edge mass [kg]	Ribs mass [kg]
Front	24512	810	1201	159
Rear	15383	745	1105	142
Vertical	-	-	-	22
Fin	-	-	100	36
Total	39895	1555	1406	359

is represented by tapered 2 nodes beam elements thus the cross section of the wing box is allowed to continuously vary along the span. For the present model, 54 CBEAM elements (Ref. [37]) have been used for the entire lifting system with approximately uniform lengths; 23 in the front wing ($1-23$, from 1 to 3 inside the fuselage), 6 in the vertical wing ($24-29$), 19 in the rear wing ($30-48$) and 6 in the fin ($49-54$). Interpolation elements (RBE3) are used to connect lumped masses to beam nodes; leading and trailing

edge masses have been also lumped on their centre of gravity. The rib masses are independently included at each end of the beam elements. The fuel mass, estimated in $79790kg$ defined in [29] according to the design mission presented in Table 3, is also lumped at the beam ends, according to cross section geometry and beam length; 61.5% is stored in the front wing and the rest in the rear one. Symmetry conditions are enforced on the wing nodes on the symmetry plane. The fin is clamped to the fuselage and to the rear wing. The connection of the fuselage to the front wing is modeled by a hinge, $3.64m$ from the centerline, that allows rotation around an axis parallel to the fuselage. The properties of beam elements have been estimated using simplified models of the wing box cross section; in this way, an approximated but natural link between mass and stiffness is obtained. Classical formulae have been used to create relationships among local design parameters and both stiffness and mass properties; their values play the role of design variables in the optimization process. The simplified models for the wing-box cross-section, are described in the next section.

Table 3
PP250 Aircraft relevant data

Description	Value
Range	6000 nm
Maximum take-off weight	230 ton
Take-off field length L_{TO}	3000 m
Takeoff airport altitude	0 m (sea level)
Landing field length L_{LAND}	$2000m$
Approach speed V_3	260 km/h
Cruise altitude	10500 m
$(T/W)_{TO}$	0.254
$(W/S)_{TO}$	575 kg/m^2
C_{D0}	0.0255
S_{REF}	$362.6m^2$

3.2. Wing cross-section models

In a first analysis, the cross section model is assumed to have a simplified rectangular shape as shown in Fig.4a and the following three parameters are considered: (i) web thickness, t_w (front and rear webs have the same thickness), (ii) skin thickness, t_s (the same for upper and lower skins), (iii) stiffener areas, A_s (the same for upper and lower box skins, reacting purely to axial forces). In conventional wing boxes in-plane bending has a minor role in structural design and the stiffness required to counteract the out-of-plane bending moment is mostly given by the upper and lower skins (plus stringers). In this case, even though the airfoil is actually not symmetric, such detail is not essential and the model can be simplified and considered symmetric with no penalization. This is no more valid for the PrandtlPlane wings: the fore and aft wing boxes experience in-plane and out-of-plane

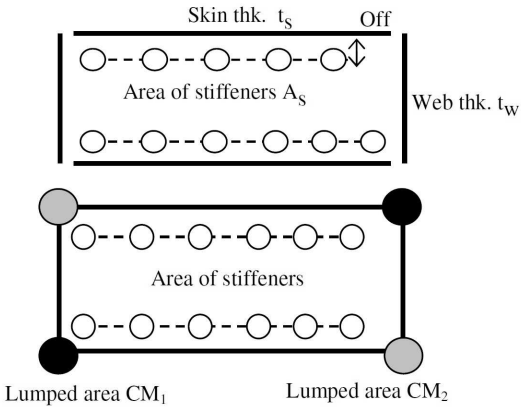

Figure 4. Schematic view of the wing box models (upper symmetric and lower asymmetric)

bending moments (Ref. [26]), a situation similar to the case of other types of joined-wing aircraft, as reported in Ref. [27]. In this case, the regions around the two corners of the rectangular box are the most stressed by the combination of the bending moments; thus it is interesting to tackle the problem of the wing structural weight estimation removing the assumption of symmetry for the wing box simplified model. In accordance with this remark, a second wing box section model is used: the external shape is again rectangular but the condition of symmetry on the section is removed by introducing two new variables in each section at the opposite corners: the areas of the spar flanges. For the sake of simplicity and calculation time reduction, they are assumed to be cross-symmetric, as depicted in Fig.4b. The principal axes of the cross section can thus rotate to account for the combination of bending moments.

Two parameters can be added to the previous ones: (i) lumped area 1, CM_1, (north-west and south-east vertex masses with the same value), (ii) lumped area 2, CM_2, (north-east and south-west vertex masses with the same value). They are considered as spar caps with L shaped section. The approach usually adopted for beam elements in Finite Element codes is maintained: the cross section stiffness of the beam is computed by multiplying a geometrical cross section parameter by a physical property of the material. Thus in the following only geometrical cross section properties are defined. The use of different materials could be addressed by adopting reference material properties (density, elastic and shear modula) and introducing appropriate weighting coefficients in the following equations. By defining the following terms: - c, h and ω the chord, the average thickness and the enclosed area of the wing box respectively; - N the number of stiffeners; - $D2$ a parameter accounting of the

mean distance, squared, of the stiffeners from the vertical neutral axis (fixed during the optimization); it is exactly evaluated, by means of number and position od stiffeners, but also approximated, by exploiting an equivalent thickness corresponding to the overall stiffeners cross section (NAs) and the chord (c) - O_{CM1} and O_{CM2} the offsets of the diagonal lumped areas CM_1 and CM_2 from the box edges - O the distance of the neutral axis of the stiffeners with respect to the wing-box skin, the equations used to evaluate the beam cross section (A), the principal moments of inertia (I_1 and I_2) and the torsional stiffness coefficient (J) of the cross section are hereafter reported as functions of the section parameters:

$$A = 2(t_s c + t_w h + A_s N + CM_1 + CM_2) \tag{1}$$

$$I_1 = 2(t_w \frac{c^2}{4} h + \frac{1}{12} t_s c^3 + A_s D_2) + \frac{1}{2} (CM_1 + CM_2) c^2 \tag{2}$$

$$I_2 = 2\left(t_s \frac{h^2}{4} c + \frac{1}{12} t_w h^3 + A_s N \left(\frac{h}{2} - O \right)^2 + CM_1 \left(\frac{h}{2} - O_{CM1} \right)^2 + CM_2 \left(\frac{h}{2} - O_{CM2} \right)^2 \right) \tag{3}$$

$$J = 2 \cdot \Omega^2 \frac{t_s t_w}{t_w c + t_s h} \tag{4}$$

By adding CM_1 and CM_2 design variables, the cross section exibits also a coupled inertia (I_{12}) given by the following Eq.5:

$$I_{12} = \frac{1}{2} \Omega (CM_2 - CM_1) \tag{5}$$

Being the cross section A_s a very practical design variable, the only design variable describing the stiffener (local effects, e.g. crippling, are not accounted for in the present optimization) scale coefficients are needed to give the actual sizes of the stiffeners, thus allowing the computation of cross section properties, in particular the position of the neutral axis. Such coefficients are defined by assuming a fixed shape and making the actual size depending on the cross section area and size ratios; we adopted a Z shape with constant thickness, a frequent design choice, so that stiffeners can be fully described by a single free parameter (the height) and two parameters size parameters: the thickness ratio, $R_t = t/D$, and the size ratio, $R_s = S/D$, as described in Fig. 5a.

A relevant driver of this model is the offsetof the neutral axis of the stiffeners with respect to the wing-box skin,O . It is derived from the stiffener cross-section by means of geometric parameters:

$$D = \sqrt{\frac{A_s}{R_t(2R_s + 1)}} \qquad O = \left(R_t + \frac{1}{2} \right) D \tag{6}$$

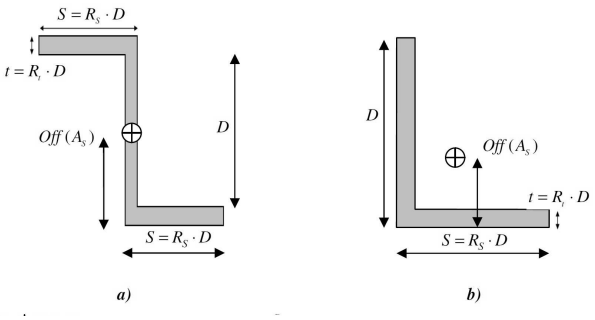

Figure 5. Conceptual shape of the stiffeners and lumped masses areas

With geometric ratios adopted in this work, i.e. $R_t = 0.12$ and $R_s = 1.0$, it leads to $O = 1.033\sqrt{A_s}$. It is modified at each step of the optimization procedure according to the modifications of the variable A_s. The use of this parameter in the calculation of the section inertia is important: it makes the optimizer sensitive to the use of panel thickness instead of stiffener area, thanks to the penalty on the stiffener contribution due to their actual positions.

The offsets of the diagonal lumped areas from the box edges, O_{CM1} and O_{CM2} , are again derived from the cap geometric modeling assumptions, a L section; also in this case two size parameters, the thickness ratio Rt=t/D and the size ratio, $R_s = S/D$ (as described in Fig. 5b) are needed to fully define the geometry starting from the height of the section. The equation for the offset computation is:

$$O_{CM} = \frac{D(1 - R_t)^2 + 2R_t (1 - R_t) + DR_t}{4 - 2R_t} D \tag{7}$$

$$D = \sqrt{\frac{A_s}{R_t(1 + R_s + R_t)}}$$

In the present case the adopted geometric ratios are $R_t = 0.085$ and $R_s = 1.0$, thus leading to $O_{CM1} = 0.6928\sqrt{A_s}$. The sensitivity analysis on these parameter is of interest but beyond the scope of the present work and delayed to a further work, where the sensitivity on local details is dealt with; nonetheless one could expect a small effect of such a local detail. A discussion on the assumptions made on some design parameters (e.g. stiffener shape, rib distance, geometric ratios Rt and Rs) could be of interest but not really necessary. They are needed to grant a design reasonably close to an actual structural solution so that the cross-section stiffness behavior is meaningful and actually feasible in a next design phase; freedom is left to the designer in finding an optimal detail design with constraints to be satisfied in terms of global stiffness but with likely different local choices.

3.3. Load conditions

Load conditions accounted for in the global design study are referred to pull-up and pull-down manoeuvers at maximum load factor (2.5 and -1.0) at the maximum speed VD. The loading pressure distribution has been computed by trimming the nominal geometry to obtain the required lift: a full three dimensional CFD code is used; this result is then translated into aerodynamic loads on the beam model by means of a proximity concept, due to the large discrepancies between the aerodynamic and structural models. The aerodynamic model too, shown in Fig.3b, is automatically generated by the procedure; 18 panels are used to discretize the chord (with cosin law used to refine the mesh at trailing and leading edges, while the span discretization follows the structural one. Static aerolasticity effects have been accounted for in terms of change in pressure distribution due to wing deflection. The change in the lift distribution on a standard wing due to structural deflection and rotation is a well known phenomenon that leads to root moment alleviation. The effects on a PrandtlPlane, composed of a positive and of a negative swept wing, with opposite behavior, are instead practically unknown, even if the presence of a wing with negative sweep could address to problems typical of such kind of wing for conventional aircraft. The different modifications on the front and rear wings originate an alteration of the internal loads, magnified by the hyper-static structure. Static aeroelasticity is introduced in the process in an iterative way: a first load calculation is carried out on the rigid wing and the weight is optimized. Once the optimized structure is obtained, the deflection due to aerodynamic loads is calculated, modifying the aerodynamic mesh accordingly.

A new load calculation is carried out with the deformed aerodynamic mesh and the optimization is restarted, accounting for the new loads. The process ends when the deflection remains the same between two consecutive steps (within a defined tolerance).

In the case of traditional aircraft configuration the iteration number is usually small, unless a very slender wing is at hand; in the present case, due to the overconstrained wing system, such number is case dependent is expected to be higher.

3.4. Objective function and constraints

The actual objective of the analysis is the simultaneous satisfaction of all the design constraints, the volume of the primary structures is used to estimate the corresponding wing-box weight and to drive the optimization algorithm to a solution in terms of minimum weight. The optimization solver is the gradient based Method of Feasible Directions implemented in SOL 200 of MSC NASTRAN38 and the constraints used are: (i) maximum stress, (ii) instability of panels and stiffeners, (iii) aileron effectiveness and (iv) flutter speed, considering the wing rigid or accounting for aeroelastic effects on load distribution.

3.4.1. Stress

In order to obtain a better estimation of the wing box weight some modifications were introduced in the stress and buckling estimation comparing to Ref. [25]. A Von Mises equivalent stress has been used so to have a reliable evaluation of the effect of multiple stress components acting simultaneously on the section: axial components are provided by NASTRAN while shear terms are evaluated by approximated equations.

Thanks to them instability of stiffened panels have been introduced while the formula for buckling of stiffeners has been replaced with the Euler-Johnson's one. Assuming that the shear forces are applied close to the shear centre and that the principal axes are close to the axes of symmetry, the shear stress on the webs and on the skins can be analytically calculated for the simplified cross section.

The axial stress due to bending is directly supplied by software at the vertices of the wing box, as standard structural response, while approximate contributions due to shear forces and torque are estimated by analytical terms, implemented in DEQATN language, so that the maximum Von Mises stress acting on webs and skins can be estimated by:

$$VM_{web} = \sqrt{\sigma^2 + 3\left(\frac{|M_t|}{2\Omega t_w} + \frac{|T_2|}{2ht_w} + k\frac{|T_1|}{2ct_w}\right)^2} \quad (8)$$

$$VM_{skin} = \sqrt{\sigma^2 + 3\left(\frac{|M_t|}{2\Omega t_s} + \frac{|T_1|}{2ct_s} + k\frac{|T_2|}{2ht_s}\right)^2} \quad (9)$$

where: M_t is the torque moment; T_1, T_2 are the shear forces along the principal axes; Ω is the enclosed area of the cross section; C and H the base and the height of the wing box, t is the local thickness and σ is the axial stress. The last term of the shear part of the equations is related to the stress flow on panels not aligned with the loads: k is a factor, set to 0.25 for webs and 0.5 for panels, accounting for the shear flow crossing the web-skin connection through the spar caps. A standard Aluminum alloy is assumed and related data, including allowable stress, obtained from (Ref. [34]), are reported in Table 1. The $233MPa$ value, lower than the yield stress, is used in order to account for different phenomena, such as local load concentration and fatigue life.

3.4.2. Instability of stiffeners and panels

Three kinds of instability are accounted for during the optimization run: the first concerns the stiffeners, the second, the portion of the panel bounded by consecutive ribs and stiffeners and the third, the whole panel bordered by ribs and webs, considered stiffened.

The critical stress is compared to the maximum compressive stress in each section. a) Euler-Johnson's formula is applied to determine the critical stress, σcr, of the stiffeners considering the effective skin width too. This equation depends on the ratio

$$\lambda = \frac{\bar{L}}{\rho} \tag{10}$$

named slenderness, and in particular on its critical value

$$\lambda_{cr} = \pi \sqrt{2 \frac{E}{\sigma_{yield}}} \tag{11}$$

Depending on the slenderness, different formulae are used:

$$\sigma_{cr} = \sigma_{yield} \left[1 - \frac{1}{4\pi^2} \frac{\sigma_{yield}}{E} \left(\frac{\bar{L}}{\rho} \right)^2 \right] \tag{12}$$

$$\sigma_{cr} = \pi^2 E \left(\frac{\rho}{\bar{L}} \right)^2 \tag{13}$$

respectively applicable when $\lambda < \lambda_{cr}$ and $\lambda > \lambda_{cr}$ and where E is Young's modulus, σ_{yield} is the yield stress, L is the effective length and ρ is the gyration radius of the stiffener accounting for the cooperating panel area; the latter is calculated using the effective width with the following equation:

$$w = tK \sqrt{\frac{E}{\sigma}} \tag{14}$$

Where the coefficient K has been settled to 1.9. From an operative point of view, Euler-Johnson's trend has been interpolated by a polynomial:

$$\begin{aligned} \sigma_{cr} = (&-3.218e-8R^5 + 1.030 - 5R^4 - 8.663e-4R^3 \\ &-3.357e-3R^2 - 1.036R + 269.334) \cdot 1e6 \end{aligned} \tag{15}$$

where R is the ratio of the distance between two consecutive ribs (assumed constant at $0.75m$) and the gyration radius of the stiffener. It has been derived from chart presented in Ref. 39.

b) The panel instability between stiffeners and ribs is calculated using:

$$\sigma_{Pcr} = \frac{\pi^2 E k_c}{12(1-\nu^2)} \left(\frac{t}{b} \right)^2 \tag{16}$$

where t is the panel thickness, E and ν are Young's and Poisson's moduli respectively, b is the distance between two consecutive stiffeners; furthermore k_c is a buckling coefficient, related to the ratio of stiffener and panel thicknesses, $r1$, and the ratio of stiffener width and b, $r2$, derived from chart presented in Ref. [39] and codified into the following equation:

$$\begin{aligned} k_c = &(23.43 \cdot r_1^2 - 24.55 \cdot r_1 + 2.22) \cdot r_2^3 + \\ &(-17.92 \cdot r_1^2 + 16.54 \cdot r_1 - 1.48) \cdot r_2^2 + \\ &(3.11 \cdot r_1^2 - 2.74 \cdot r_1 + 0.24) \cdot r_2 + \\ &(-6.69 \cdot r_1^2 + 13.17 \cdot r_1 - 1.24) \end{aligned} \tag{17}$$

c) The global instability of the stiffened panels between the webs and ribs is calculated using:

$$\sigma_{Pcr} = \frac{\pi^2 E k_2}{12(1-\nu^2)} \left(\frac{t}{b} \right)^2 \tag{18}$$

where k_2 is the buckling coefficient of the stiffened panels. It depends on the ratio $r2$, previously described, and on the parameter $r_3 = 12I(1-\nu^2)/(bt^3)$ whose term I is the equivalent sectional inertia of the stiffener considering the contribution due to the collaborative area of the panel. From an operative point of view, the following interpolation equation, again derived from Ref. [39], has been used:

$$\begin{aligned} &c_1 = 4.4396 - 1.8146 \cdot r_2 + 0.0895 \cdot r_3 + 0.1708 \cdot {r_2}^2 - \\ &0.0104 \cdot r_2 \cdot r_3 + 3.2538e-6 \cdot r_3^2 \qquad c_2 = 4 \\ &k_2 = \min(c_1, c_2) \end{aligned} \tag{19}$$

3.4.3. Aileron effectiveness

The incremental load due to aileron deflection and the change in chord pressure distribution, can induce a change in wing geometry and in airfoil attitude, and may thus possibly lead to a reduction of the lifting forces, with a consequent loss of efficiency. A positive sweep angle reduces the aileron efficiency due to bending; the opposite occurs for a negative sweep angle. It is to be noted that PrandtlPlane wings allow to position the ailerons on the rear negative swept wing or to split them between the front and rear wings. In the present case, according to Ref. [29], the aileron has been placed on the rear wing and spans a length of $9.25m$ from the tip. The roll effectiveness is evaluated according to Ref. [25] as:

$$\eta = 1 - \frac{\Delta M_{Roll}}{M_{Rigid\_Roll}} \tag{20}$$

where Δ_{Roll} is the change in rolling moment due to the structural flexibility and M_{Rigid_Roll} is the nominal rolling moment assuming the nominal geometry, i.e. a rigid structure. The two terms are computed according to the procedure described in cited reference. The effectiveness can be constrained according the values for flexible wings at high speed: in the present case, a value of 0.525, reasonable for such application, has been chosen at $460km/h$.

3.4.4. Flutter speed

The airplane must prove to be flutter free in the flight envelope enlarged by 15%. FAR regulations

state that the calculations for flutter speed must be based on equivalent air speed: the following calculations take this into account. The design constraint Vmax, the velocity below which no flutter should occur, has been defined according to the worse of the following flight conditions: 1) At the cruise altitude of $10500m$, the calculation is based on the Mach number, as it is the limiting parameter. The cruise Mach number being MC =0.85, the design dive Mach number at cruise altitude is computed as $M_D = M_C + 0.05 = 0.90$, meaning a diving speed $V_D = 267.55m/s$, True Air Speed (TAS). Considering the EAS, one obtains $V_D = 150.52m/s$ and, enlarging the flight envelope by 15%, one obtains $V_{max} = 173.1m/s$. 2) At sea level, the diving speed is directly computed from the cruise velocity. According to Ref. [40], this point for jet aircrafts is generally situated at altitudes between 20000 and $25000ft$. Considering the most constraining case, at $20000ft$, one obtains, for a cruise Mach number $M_C = 0.85$, a cruise velocity $V_C = 268.63m/s$ TAS.

Taking the EAS one obtains $V_C = 196.08m/s$ and the diving speed is $V_D = 1.25V_C = 245.10m/s$. Again enlarging the flight envelope by 15%, one obtains $Vmax = 281.87m/s$. The flutter analysis must then show that no flutter occurs before the speeds determined above; thus it has been executed at a fixed altitude (0 m) and fixed Mach number (0.8) up to the maximum velocity $V_{max} = 282m/s$ as a subcase of the optimization process.

4. Results

4.1. Three parameter wing box model

The optimization process was applied in the case of a wing box defined by the three previously discussed parameters (web and skin thickness and stringer area) for a total of 162 design variables. The different design constraints are applied successively so that it is possible to single out their influence on the structural design; the different cases considered are the following:

Case A: Constraint on maximum stress. From previous experience, the maximum stress has been set to $233MPa$ at the limit load factor of $n = 2.5$. Case B: Same as Case A, with an additional constraint on the instability of the stiffeners and panels. Case C: Same as Case B, with an additional constraint on aileron effectiveness. The minimum aileron effectiveness was chosen to be higher than 52% of the rigid case, according to a reasonable performance decay. Case D: Same as Case C, accounting for static aeroelastic effects on load distribution; indeed this point is not a design constraint but it is needed to assess the validity of the assumption on load distribution Case E: Same as Case D, with the additional constraint on flutter speed.

Table 4 shows the influence of the previously described constraints on the weight of the different parts of the wing. The weights presented are for half of the lifting system. The total wing weight of the lifting system and fins includes the weight of the wing box as well as the weights of the leading and trailing edges and the ribs; fuel is not included.

These results need further comments. First, the addition of the constraint on the instability of panels and stiffeners seems to be severe, particularly for the vertical wing: the stress state in the vertical wings includes in-plane and out-of-plane components deriving from vector decompositions of the stress characteristics in both the horizontal wings and it also contains severe compression stresses. The fin also suffers from this constraint, although with a smaller increase in weight. The constraint on the aileron effectiveness does not require any additional weight: the particular geometry of the lifting system, with the ailerons mounted on the negative sweep wings, offers high aileron efficiency. Static aeroelastic effects on the load redistribution are beneficial for the front wing and unfavorable for the rear wing due to the sweep angles. Front wing lift is reduced due to out-of-plane bending and torsion coupling that generates lower angles of attack; the opposite happens on the rear wing, where bending increases the local angle of attack and, consequently, local aerodynamic loads. The trends of the lift distribution, on the front and rear wing, in the rigid and aeroelastic cases, are shown in Fig. 6. Taking all the

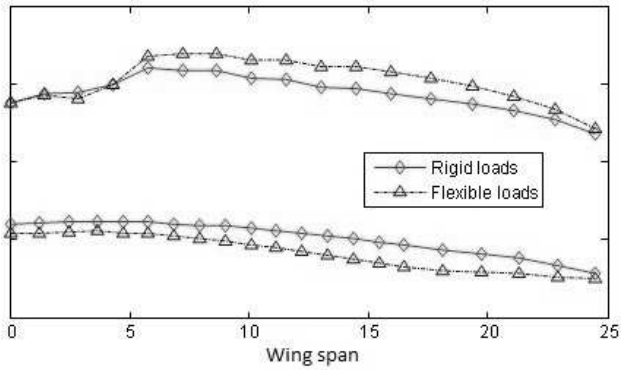

Figure 6. Lift distribution on front (lower) and rear (upper) wings with nominal and deflected geometry

previous effects into account, the front wing weight decreases wherea s the rear wing experiences an increase in weight and the overall result can be summarized in a 2.6% increase in the total wing box weight as compared to Case B. The centre of gravity of the entire wing, including the fuel, moves back by $1.16m$ for Case D with respect to Case B, ending up at $27.43m$ from the root leading edge of the front wing.

The optimized behavior presents high torsion and bending stiffnesses and thus the flutter constraint is inactive. The trends of the optimized variables along

Table 4
Influence of the constraints on wing component weights (symmetric wing box)

	Case A	Case B	Case C	Case D	Case E
Front kg	5313	5837	5837	3845	4065
	-	(9.9%)	(0.0%)	(-34.1%)	(5.7%)
Vertical kg	500	617	617	638	684
	-	(23.4%)	(0.0%)	(3.5%)	(7.1%)
Rear kg	5776	6405	6405	8914	8755
	-	(10.9%)	(0.0%)	(39.2%)	(-1.8%)
Fin kg	1000	1167	1167	1471	1411
	-	(16.7%)	(0.0%)	(26.0%)	(-4.1%)
In fuselage kg	1345	1414	1414	978	996
	-	(5.1%)	(0.0%)	(-30.8%)	(1.8%)
Total box kg	13936	15442	15442	15848	15911
	-	(10.8%)	(0.0%)	(2.6%)	(0.4%)
Total wing kg	18255	19761	19761	20167	20231
	-	(8.3%)	(0.0%)	(2.1%)	(0.3%)

The relative change is computed with respect to the previous column

the span are compared in Fig. 7, 8 and 9. Comparing the trends of the variables in the different constraint cases, it becomes evident that the results of Case A are unrealistic. The stiffener area is maintained at the minimum technological limit ($80mm^2$) whereas the skin thickness reaches its maximum. This effect is due to the lower efficiency with respect to axial stresses of the mass of the stiffeners with respect to skin panel: due to the offset, the stringer centre of gravity is closer to the neutral axis of the wing box and thus its contribution to sectional inertia diminishes; so the optimization algorithm prefers to move material to the panels. Consequently, for the wing box model adopted, it is essential to introduce instability constraints in order to recover the correct contribution of the stiffeners to the total mass.

A clear difference is visible between the results of Case A and Case B as compared to Case D and Case E. Whereas the first two are related to the rigid wing, the second two concern the flexible wing: the front wing shows a strong reduction in thickness, for both webs and skins, passing from the rigid to the elastic case. Complementary effects are shown by the rear wing. It is thus evident that, in order to obtain reliable solutions, the static aeroelastic behavior of the PrandtlPlane cannot be left aside during the preliminary design, even though this implies an important increase in calculation time.

Web thickness presents suspect values in the fin: at the joint with the rear wing it reaches values of about $70mm$. This increment is probably due to a stress concentration that comes from modeling simplifications: the actual design of the details is fundamental for stress alleviation. Further investigation in this direction is planned.

In synthesis: the optimal solution uses very thick panels that are preferred to stiffeners due to their influence on both bending and torsional inertia. The stiffener area is maintained at a minimum due to the influence of offset, but it does not reach the technological limit because the instability constraint becomes active. The output of the optimization code includes many information about the wing structure, which is very different from that of a conventional wing. Let us consider the internal loads at the maximum positive load factor ($n = 2.5$). As known in a cantilever wing the bending moment is null at the tip, whereas in the case of a PrandtlPlane this happens before reaching the ends of both the front and rear wings (approximately at 75% of the wing span). In this way, the maximum bending moment at the wing root is lower than for a traditional aircraft, under the same total lift. The bending moment distribution on the rear wing is clearly influenced by the presence of the fin and, in order to reduce empty weight, the design features a maximum distance between the two fins. It's important to emphasize that in this unconventional wing configuration, the in-plane bending moment assumes values comparable to the out-of-plane one, and the trend of the internal loads, due to the fact that the structure is statically undetermined, depends on the structural actual sizing. The effect of static aeroelasticity is also clearly shown in Fig.10: the aerodynamic load rearrangement causes, in Case D and Case E, a strong decrease of the bending moment in the front wing and an increase in the rear one, which leads to a relocation of the structural material between the two lifting surfaces. On the vertical wing, the out-of-plane bending moment (Fig.11) is zero at about half of the length, which reflects the butterfly-shaped lift distribution necessary for the minimum lift condition.

Figure 12 shows the trend of the area, out-of-plane, in-plane and torsional inertias of the optimized sections in the front and rear wings. It is important to note that the rear wing, although with a greater amount of structural material, has a smaller out-of-

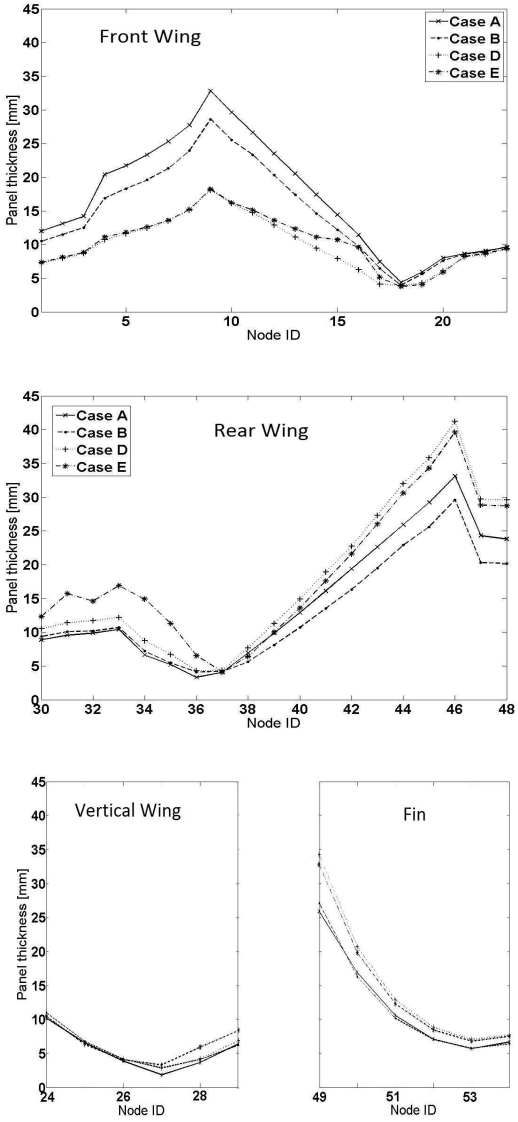

Figure 7. Skin thickness along the span (symmetric box model)

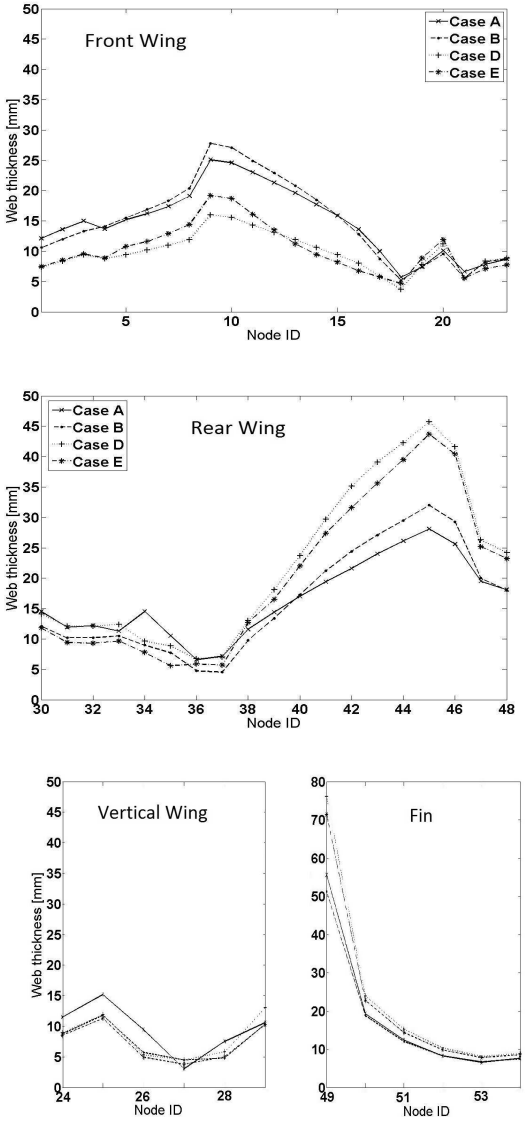

Figure 8. Web thickness along the span for the symmetric box

plane, in-plane and torsional inertia with respect to the front one, due to the smaller thickness of the rear wing airfoils. It is possible to foresee that an increase in the rear wing airfoil thickness will produce a relevant reduction on the overall weight, although its impact on flight mechanics has to be analyzed.

Eigenmode shapes and frequencies can be easily obtained using the optimized stick model, e.g. with the SOL 103 of MSC NASTRAN; they are reported, for Case E, up to $5Hz$, in Table 5 and in Fig. 13. The first mode, with a fairly low frequency of $0.75Hz$, is principally a quarter wavelength bending mode, where the front and rear wings are moving in phase. The node for the front wing is situated at the junction with the fuselage, whereas the node for the rear wing is situ-

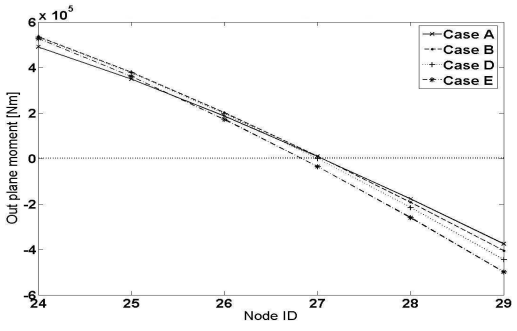

Figure 11. Out of plane bending moment for the vertical wing(n=2.5)

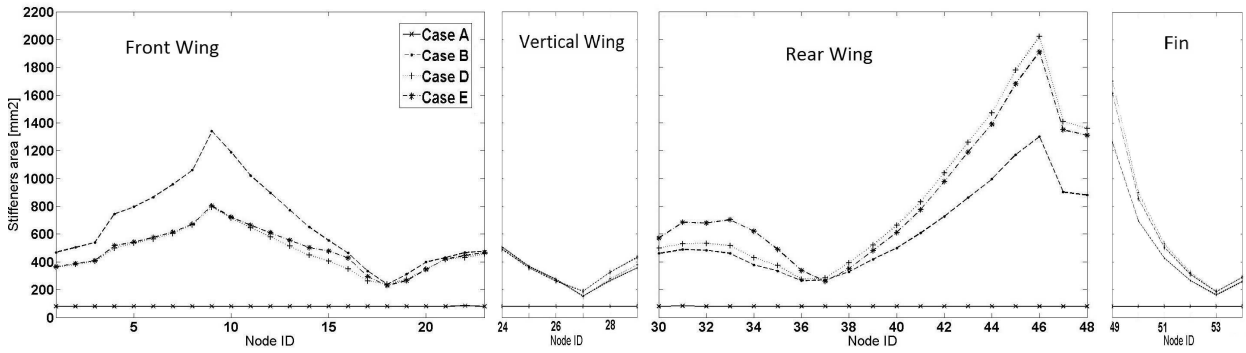

Figure 9. Stiffener area along the span for the symmetric box

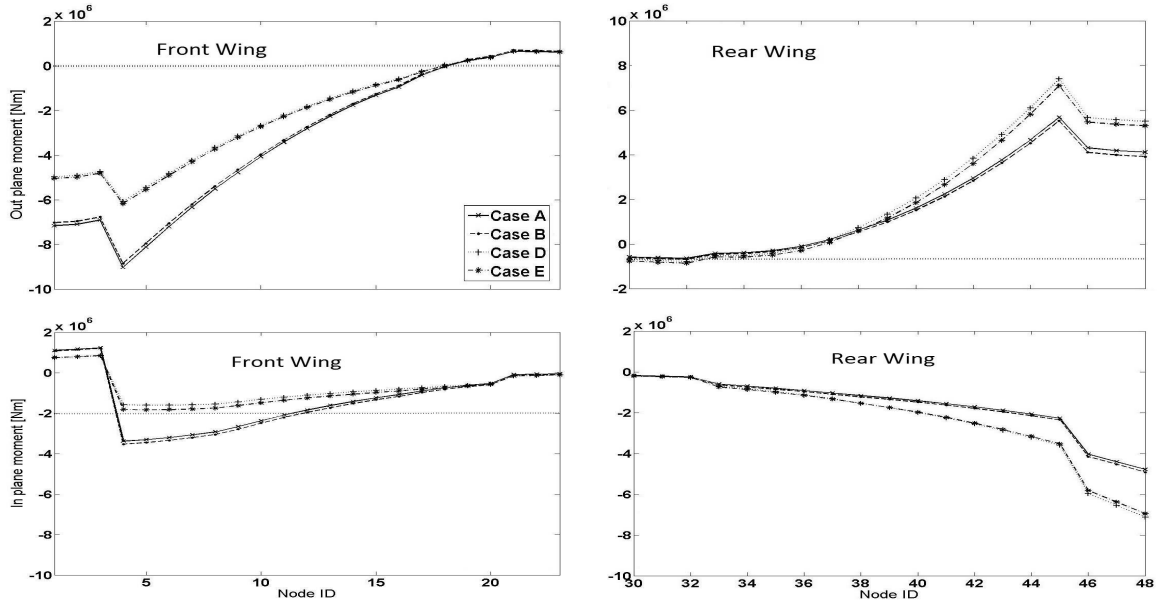

Figure 10. Bending moment comparison along the wing span: out-of-plane (upper) and in-plane (lower) (n=2.5)

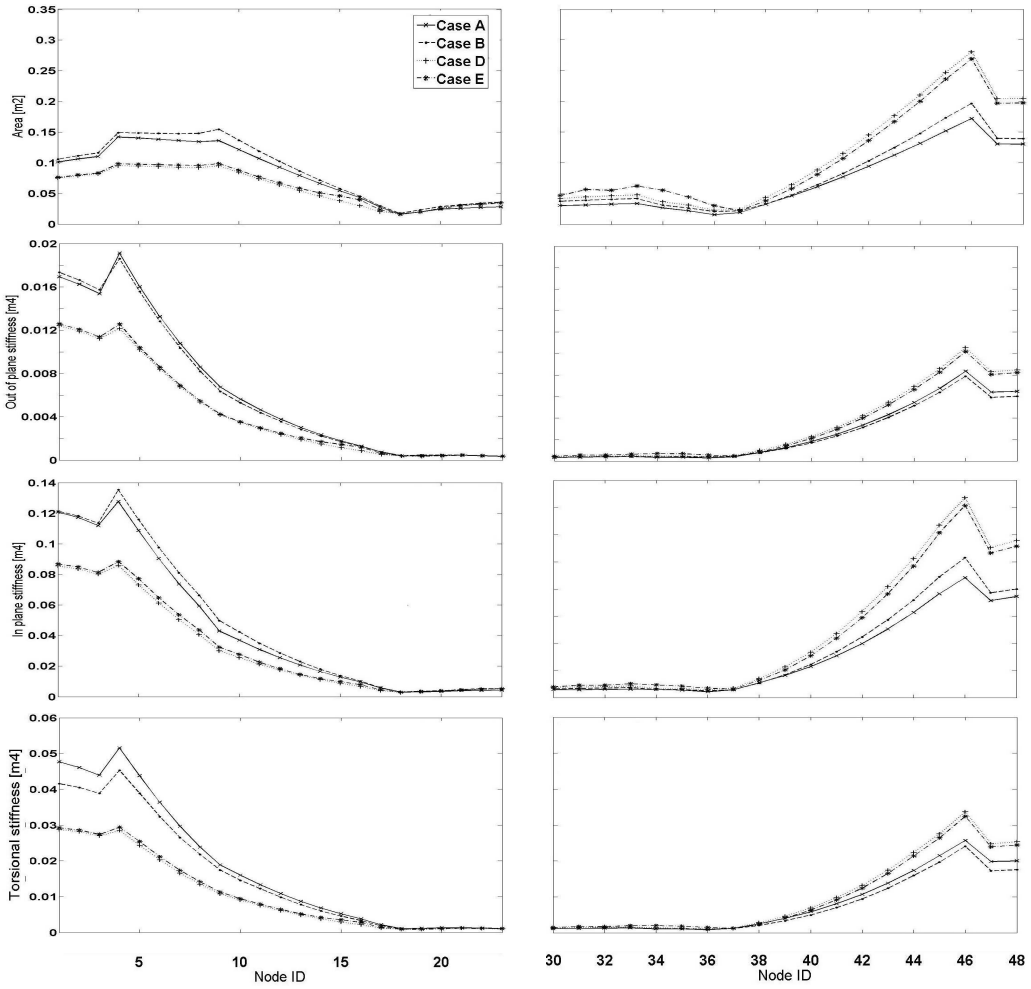

Figure 12. Sectional inertia along front (left) and rear (rught) wings

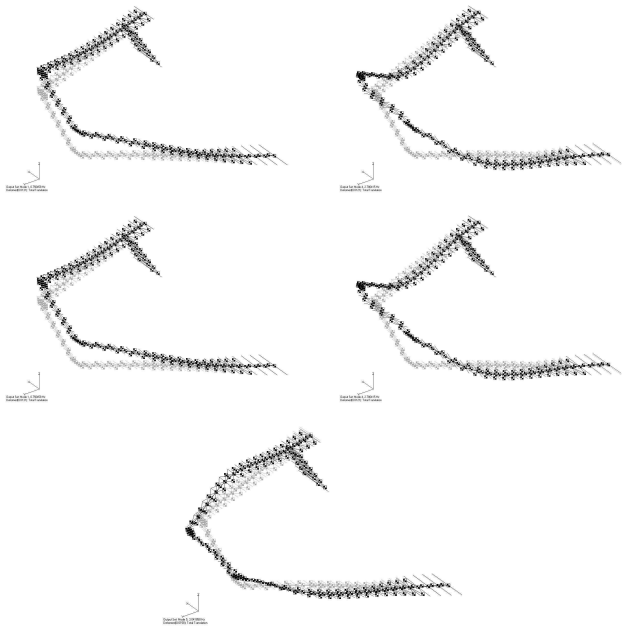

Figure 13. Mode shapes for the PP250 (Case E)

ated at the connection with the fin; this causes the vertical wing to oscillate vertically, parallel to its equilibrium position. In the second mode, the bending of the two wings is also of a quarter wavelength, but the two wings move in opposition of phase. This causes the vertical wing to rotate around a point situated at about a third of its span, closer to the front wing. The vertical wing is thus working in compression, without significant deformation; consequently, a non negligible amount of in-plane deformation is introduced on both wings in such a way that, when the front wing moves forwards, the rear wing moves backwards and vice-versa. The third mode exhibits a half-wavelength bending deformation; the nodes are, in addition to the two already cited, situated at the wing-tips; the vertical wing moves parallel to itself, following a quasi horizontal axis.

Here too, the in-plane deformations are significant, but the two wings are moving in phase.

Similarly to the situation encountered in the first mode, in the fourth mode the vertical wing is vertically translating parallel to itself. The bending shape of the wings however exhibits a half wavelength; in-plane deformation is also not negligible. The behavior observed is similar to that of the third mode, where the two wings move in phase. The fifth mode shows a behavior analogous to the second mode; the vertical wing rotates around a point, and the in-plane movements of the wings are out-of-phase; the bending shape exhibits slightly more than a half wavelength, the nodes being at around 6m from the wing tips on each wing. We can remark that, for the first five modes, neither the fin nor the vertical wing deform in bending.

Table 5
Wing modes

Mode #	Freq. (Hz)	Description
1	0.75	in-phase quarter wavelength bending of the two wings (no in-plane deformation)
2	1.46	out-of-phase quarter wavelength bending of the two wings (out-of-phase in-plane deformation)
3	2.17	in-phase half wavelength bending of the two wings (in-phase in-plane deformation)
4	2.79	in-phase half wavelength bending of the two wings (in-phase in-plane deformation)
5	3.04	out-of-phase half wavelength bending of the two wings (out-of-phase in-plane deformation)

These structural elements work in bending only at higher frequencies which, from these preliminary results, seem of no interest for flutter.

4.2. Four parameter wing box

The introduction of the asymmetric wing box model leads from 162 to 270 design variables with a relevant increase in computational time. In order to correctly account for the asymmetry of the section and also avoid an unmeaning rotation of the principal axes, Case A has been modified, introducing the $n = -1$ load case alongside the $n = 2.5$ aerodynamic loads. In fact, when using only the positive load factor, the inertial axes undergo a very large rotation; even though the wing box obtained is perfectly able to satisfy the needs of this case, it becomes unfeasible for the negative load factors because of the increased distance of the spar caps from the neutral axis. Table 6 shows the influence of the constraints on the weight of the different parts of the wing using the asymmetric wing box model. Weights are still presented for half of the lifting system. The introduction of the alternative wing box layout allows to save about $2100kg$ on the final wing weight, Case E, that leads to a reduction of the structural weight estimate of about 12.5%.

The following figures report the most significant results, limited to the front and rear wings, in the presence of static constraints, instability, roll and flutter (Case E) for the symmetric and asymmetric wing boxes. The area of the wing box sections along the span are presented in Fig. 14, which summarizes the previous results. It shows that the volume saving, thanks to the introduction of the asymmetric model, is significant along the entire span but it is especially remarkable between the root and about 2/3 of the span for the front wing. In the rear wing, the weight saving is more significant between the root and about half of the span. Due to the introduction of the concen-

Table 6
Influence of the constraints on the wing component weights (asymmetric box)

	Case A	Case B	Case C	Case D	Case E
Front kg	4425	4701	4701	3362	3360
	-	(6.2%)	(0.0%)	(-28.5%)	(-0.1%)
Vertical kg	662	814	814	842	842
	-	(23.0%)	(0.0%)	(3.4%)	(0.0%)
Rear kg	5039	5502	5502	7277	7298
	-	(9.2%)	(0.0%)	(32.3%)	(0.3%)
Fin kg	984	1152	1152	1477	1471
	-	(17.0%)	(0.0%)	(28.3%)	(-0.4%)
In fuselage kg	1228	1304	1304	933	928
	-	(6.2%)	(0.0%)	(-28.5%)	(-0.1%)
Total box kg	12338	13472	13472	13891	13898
	-	(9.2%)	(0.0%)	(3.1%)	(0.1%)
Total wing kg	16657	17791	17791	18209	18217
	-	(6.8%)	(0.0%)	(2.4%)	(0.0%)

The relative change is computed with respect to the previous column

trated lumped masses at the vertices of the sections, the principal axes of the sections rotate with respect to a reference system aligned with the side of the rectangular wing box. In order to easily compare the behavior of the bending moments for the symmetric and asymmetric sections, they are all plotted referring to the original axes, whereas the trend of the static inertia, I_{12}, is shown in a separate graph. The out-of-plane inertia of the front and rear wings is presented in Fig. 15; it appears that the optimal asymmetric box section allows only a small reduction of the bending inertia, concentrated, for both wings, in proximity of the fuselage. The difference is instead negligible for

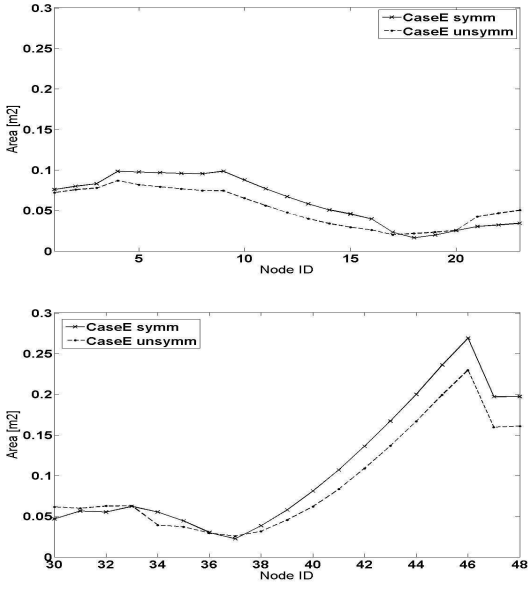

Figure 14. Comparison of the wing box area for the symmetric and asymmetric model: front (a) and rear (b) wing

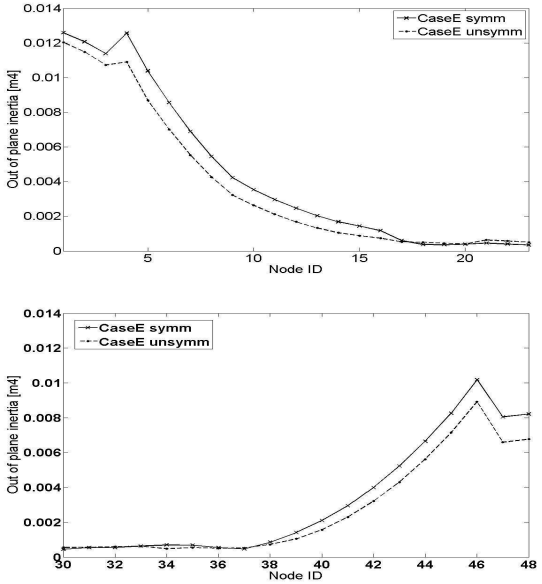

Figure 15. Comparison of the wing box out-of-plane inertia for the symmetric and asymmetric models): front (upper) and rear (lower) wings

the in-plane bending moment, thus it is not reported.

The asymmetric wing box model allows the rotation of the sectional neutral axes acting in a differential way on the diagonal lumped masses. The change in the position of the neutral axes generates a decrease of the maximum stress in the section with a consequent reduction of weight. Fig. 16 shows the principal axes rotation angle allowed by the asymmetric model. Even though the rotation of the principal axes is limited, its benefits are relevant, as proved by the significant decrease in total weight. On the other hand, the torsional stiffness is reduced by the introduction of the asymmetry of the section. For the front and rear wings, the reduction is important in the sections from the root to half of the span, as shown in Fig. 17. The difference

between the section inertias derives from the reorganization and modification of the material used in the stringers, caps, webs and skins to resist to the stress. In fact, the additional masses, simulating the caps of the spars placed at the corners of the rectangular wing box, have a great impact on the section layout, due to the high distance from both of the neutral axes, inducing a complete rearrangement of all of the other structural components. It is evident that the intro-

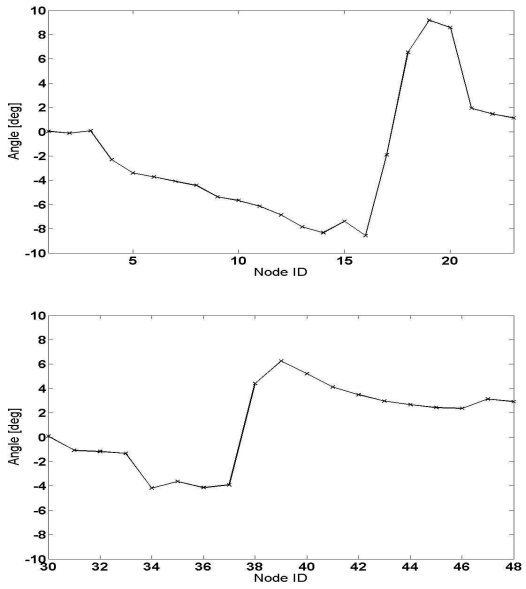

Figure 16. Rotation of the neutral axes for the asymmetric model (Case E): front (upper) and rear (lower) wings

duction of the two new variables does not allow a direct comparison of the data, especially for the stiffeners: to bypass this problem, Fig. 18 shows, for the asymmetric model, the equivalent areas of the stringers and lumped masses. The use of the asymmetrical wing box introduces a relevant increase in the influence of the longitudinal components in the kinky part of the front wing, whereas in the tip zone, this increase is limited. On the other hand, for the rear wing, the asymmetric solution presents a more uniform increment, reaching its maximum near the root.

The asymmetrical wing box model has the opposite effect on skin thickness, as can be seen in Fig. 19. The first graph, concerning the front wing, shows the great weight saving along the entire span but, more significantly, up to 16m span; the thickness reduction is of $7mm$ around the end of the kink. A great advantage is obtained on the rear wing as well, second graph, with a maximum of 9 mm at the fin intersection. Fig. 20 refers to the last optimization variable, the front and rear web thickness. The thickness reduction, about $7mm$, due to the introduction of the asymmetrical model is very evident in the kink zone

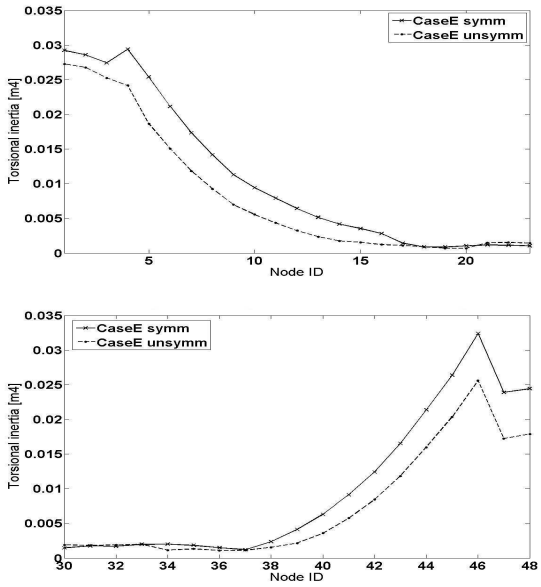

Figure 17. Comparison of the wing box torsional inertia for the symmetric and asymmetric models: front (upper) and rear (lower) wings

of the front wing. On the rear wing, the difference between the two cases is strong, maintaining a reduction of about 8mm throughout the inner part of the wing.

In Figs. 21 the height of longitudinal elements, i.e. stiffeners and flanges (CM_1 and CM_2) are depicted to offer a physical insight into the possible guess sizing produced by the weight estimator. The thicknesses are not represented being related to the height by the geometric ratios previously defined. It's worth to observe that the sizes are fully compatible with a classical sizing of such structural components, despite they are due to the need of a rotation of the cross section principal axis.

5. Comparison between standard and Prandtl Plane configurations

A validation of the method employed has been presented for conventional wings in Ref. [25]. The obtained weight estimation of B747-100 was compared with available data and values obtained by other statistical methods with a satisfactory matching. A comparison between the weights of the PrandtlPlane wing and a conventional one has been carried out in order to estimate the impact of the new configuration on the weight of the primary structures. Three airplanes, comparable in terms of maximum take-off weight and mission range, have been chosen. In order to normalize the differences, the ratio between wing and take-off weight has been adopted as a figure of merit. The wing masses of the A330-300, B767-300 and B777-300 are not directly known and are thus extrapolated using an analytical/statistical procedure, described in Ref. [34], whereas the other data and the necessary geometri-

Table 7
Aircraft data and Wing weight comparisons

	A330-300	B767-300 ER	B777-300	PP250
Range, nm	5'669	5'990	6'005	6'000
WTO, kg	230'000	186'880	299'370	230'000
Wing Span	67.3	47.6	67.9	52.0
Overall Length m	63.7	54.9	73.9	47.0
Passengers (3 classes)	295	218	386	329
Fuselage diameter m	5.64	5.03	6.20	7.3
Max Fuel Capacity l	97'500	91'400	171'000	95'000
Wwing, kg	33'697	24'293	47'671	33'494
Wwing + tail, kg	37'067	26'722	52'438	36'435
Wwing/WTO, %	14.7	13.0	15.9	14.6
Wwing + tail/WTO, %	16.1	14.3	17.5	15.8

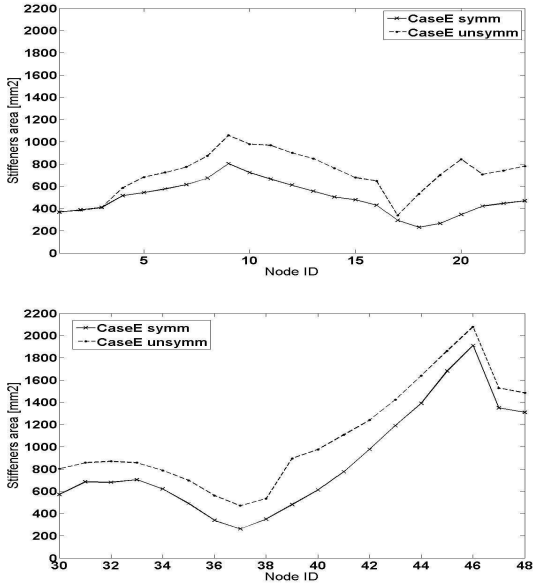

Figure 18. Comparison of the stiffener areas for the symmetric and asymmetric models: front (upper) and rear (lower) wings

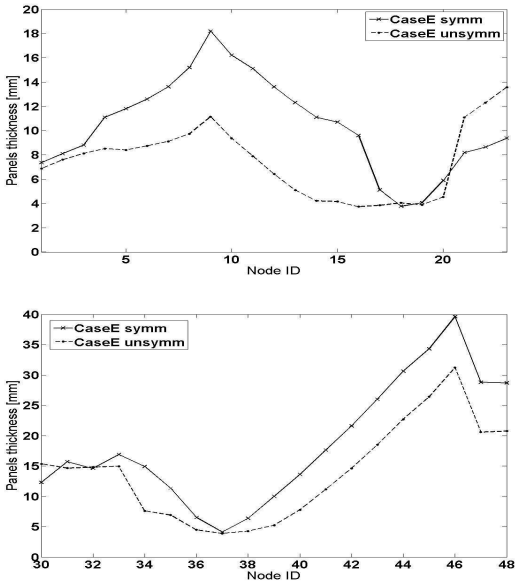

Figure 19. Comparison of the panel thicknesses for the symmetric and asymmetric models: front (upper) and rear (lower) wings

cal information have been found in Ref. [41]. The tail weight, including horizontal and vertical units, has been estimated to be 10% of the wing weight, according to literature, for the standard configuration airplane while, for the Prandtl Plane, the weight of the fins has been simply added. The results are summarized in Table 7. Although a final answer cannot be given due the approximations adopted and the differences between the aircraft used for the comparison, the PrandtlPlane configuration is comparable, in terms of wing structural efficiency, to the standard solution.

6. Conclusions

A previously developed weight estimator for wingbox systems has been improved to approach unconventional aircraft configurations. It has been assessed in the case of a PrandtlPlane unconventional aircraft: weight and cross section inertia properties have been obtained. Constraints concerning stress, instability, aileron effectiveness and flutter have been considered in order to achieve a better reliability of the results obtained, even in such preliminary phase of the design.

Aeroelastic static effects on aerodynamics have also been taken into account. The procedure adopted has shown the differences between a standard wing and the present one: a completely different distribution of the internal loads along the span and the presence of an in-plane moment comparable in terms of magnitude to the out-of-plane one has been confirmed; a different aeroelastic behavior of the front and rear wings, due to the positive and negative sweep angles, has also been outlined. The literature alternative model of the wing section has been considered and implemented in order to minimize the effect of aprioristic assumptions, such as wing box symmetry, able to significantly bias the results. The soundness of the idea of allowing the rotation of the neutral axis has been confirmed. The

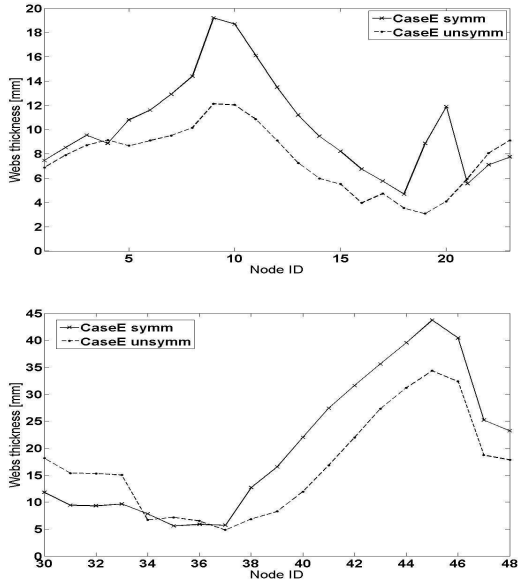

Figure 20. Comparison of the web thicknesses for the symmetric and asymmetric models: front (upper) and rear (lower) wings

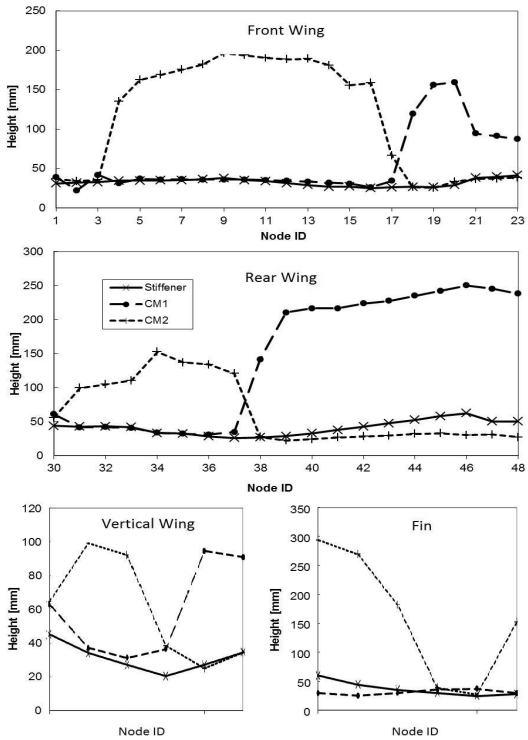

Figure 21. Flanges (CM_1 and CM_2) and stiffeners cross section height

PrandtlPlane wing has been compared to that of other conventional liners whose weights were evaluated by classical semi-empirical methods. These results show that the prediction of mass needed for the lifting system of the PP250, in percentage of MTOW, is consistent with that of current aircraft. An improvement in effectiveness can probably be reached by coupling the aerodynamic and structural design by MDO techniques that would almost certainly increase the rear wing airfoil thickness, diminishing the material while maintaining sectional inertia. Further studies will investigate the weight reduction with the use of composite materials and the effects of the introduction of further design constraints, e.g. the gust load, on wing-box weight prediction and design variables distribution.

REFERENCES

1. P. Busquin, et Al., European Aeronautics: A Vision for 2020. European Community, Bruxelles, Jan. 2001.
2. Anonymous,'Vision 2020: Strategic Research Agenda, Volume 1.'Advisory Council for Aeronautics Research in Europe (ACARE), Oct. 2002.
3. I. M. Kroo,'Nonplanar Wing Concepts for Increased Aircraft Efficiency', Von Karman Institute, Lecture Series on Innovative Configuration and Advanced Concepts for Future Civil Aircraft, Jun. 2005.
4. I. M. Kroo, J. H. McMasters, and S. C. Smith,'Highly Nonplanar Lifting System',Tech. Rep., NASA, Sept. 1995.
5. I. M. Kroo,'A General Approach to Multiple Lifting Surface Design an Analysis', AIAA 84–2507, Oct. 1984.
6. A. Frediani,'The Prandtl Wing',Von Karman Institute, Lecture Series on Innovative Configuration and Advanced Concepts for Future Civil Aircraft, Jun. 2005, Lecture series VKI, 2005–06, pp.1–23
7. E. Torenbeek,'Introductory Overview of Innovative Civil Transport Aircraft Configurations.'Von Karman Institute, Lecture Series on Innovative Config. and Advanced Concepts for Future Civil Aircraft, Jun. 2005.
8. J. H. McMasters and I. M. Kroo,'Advanced Configuration for Very Large Transport Airplanes.'Invited AIAA paper 1998–0439, 1998.
9. A. Frediani, E. Rizzo, C. Bottoni, J. Scanu, and G. Iezzi,'The PrandtlPlane Aircraft Configuration',in Aeronautics Days, (Wien), Jun. 2006. Delft University of Technology 73
10. W. Schneider,'The Importance of Aerodynamics in the Development of Commercial Successful Transport Aircraft',in Notes on Numerical Fluid Mechanics (Springer, ed.), vol. 76, Peter Thiede, 2000.
11. J. H. McMasters, et Al.,'Advanced Configuration for Very Large Subsonic Transport Airplanes',Contractor Report 198351, NASA, Oct. 1996.
12. Wolkovitch J. The joined wing: an overview. J Aircr 1986; 23: 161–178.
13. Kroo I, Gallman JW and Smith SC.'Aerodynamic and structural studies of joined-wing aircraft'. J Aircr 1991; 28(1): 74–81.
14. Nangia RK, Palmer ME, and Tilman CP.'Unconventional high aspect ratio joined-wing aircraft with aft and forward swept wing tips'. In: Proceedings of the 41st Aerospace sciences meeting, Reno, Nevada,6–9 January 2003, paper no. AIAA-2003-0605.
15. Addoms RB and Spaid FW.'Aerodynamic design of high performance biplane wings'. J Aircr 1975; 12(8): 629–630.
16. Lin H, Jhou J, and Stearman R.'Influence of joint fixity on the structural static and dynamic response of a joined-wing aircraft'. In: Proceedings of the 31st AIAA/ASME/ASCE/AHS/ASC Structures structural dynamics and materials conference, Long Beach, CA, 2–4 April 1990. Reston, VA: American Institute of Aeronautics and Astronautics, paper no. AIAA 90-0980.
17. Bagwell T. and Selberg B.'Aerodynamic investigation of joined wing configurations for transport aircraft'. In Pro-

ceedings of the 14th Applied aerodynamics conference, NewOrleans, LA, 17–19 June 1996. Reston, VA: American Institute of Aeronautics and Astronautics, paper AIAA no. 96-2373.
18. Hajela P.'Weight evaluation of the joined wing configuration'. Washington, DC: NASA, report no. CR-166592, June 1984.
19. F. Hürlimann, R. Kelm, M. Dugas, K. Oltmann, G. Kress;'Mass estimation of transport aircraft wingbox structures with a CAD/CAE-based multidisciplinary process'; Aerospace Science and Technology, Volume 15, Issue 4, June 2011, Pages 323-333
20. F. Hürlimann, R. Kelm, M. Dugas, G. Kress;'Investigation of local load introduction methods in aircraft pre-design', Aerospace Science and Technology, Volume 21, Issue 1, September 2012, Pages 31-40
21. James Ainsworth, Craig Collier, Phil Yarrington3, Ryan Lucking and James Locke;'Airframe Wingbox Preliminary Design and Weight Prediction', 69th Annual Conference, Virginia Beach, Virginia, 05/2010, Virginia Beach, Virginia, 2010, p.41
22. Franco Mastroddi, Marco Tozzi, Valerio Capannolo;'On the use of geometry design variables in the MDO analysis of wing structures with aeroelastic constraints on stability and response'; Aerospace Science and Technology, Volume 15, Issue 3, April–May 2011, Pages 196-206
23. Heiko Engels, Wilfried Becker, Alan Morris;'Implementation of a multi-level optimisation methodology within the e-design of a blended wing body'; Aerospace Science and Technology, Volume 8, Issue 2, March 2004, Pages 145-153
24. Paul O Jemitola, Guido Monterzino, John Fielding and Craig Lawson,'Tip fin inclination effect on structural design of a box-wing aircraft', J. of Aerospace Engineering, Published online before print Jan 5, 2012, doi: 10.1177/0954410011426528
25. G. Bindolino, G. Ghiringhelli, S. Ricci, and M. Terraneo,'Multilevel Structural Optimization for Preliminary Wing-Box Weight Estimation', Journal of Aircraft, vol. 47, No. 2, pp. 475–489, Mar.-Apr. 2010.
26. G. Ghiringhelli, S. Ricci,'A Multi-Level Approach to Preliminary Optimization of a Wing Structure', Int. Forum on Aeroelasticity and Structural Dynamics IFASD 2001, 5-7 June 2001 - Madrid (Spain)
27. Hajela, P., and Chen, J.,'Preliminary Weight Estimation of Conventional and Joined Wings Using Equivalent Beam Models'Journal of Aircraft, Vol. 25, No. 6, 1988, pp. 574–576.
28. C. Bottoni and J. Scanu,'Preliminary Design of a 250 Passenger PrandtlPlane Aircraft',Master's thesis, Università di Pisa, Facolta di Ingegneria, 2004.
29. G. Iezzi,'PrandtlPlane High Lift System Preliminary Aerodynamic Design',Master's thesis, Università di Pisa, Facolta di Ingegneria, 2006.
30. H. Miura and A. Shyu,'Weight Estimation of Unconventional Structures by Structural Optimization', SAWE Paper No. 1718, May 1986
31. J. Sobieszczanski-Sobieski e R. T. Haftka,'Multidisciplinary Aerospace Design Optimization: Survey of Recent Development', Structural Optimization, 14(14): 1-23, 1997, Review article
32. T.Klimmek, F.Kiebling and H.Honlinger,'Multidisciplinary Wing Optimization Using a Wing Box Layout Concept and Parametric Thickness Model', 9th AIAA Symposium on Multidisciplinary Analysis and Optimization, AIAA-2002-6757, Atlanta, GE, Sept. 4-6, 2002
33. J. Sobieszczanski-Sobieski, B. James e A.R. Dovi,'Structural Optimization by Multi-Level Decomposition', AIAA Journal, Vol.23, No.11, November 1983
34. E. Torenbeek,'Development and Application of a Comprehensive Design-Sensitive Weight Prediction Method for Wing Structures of Transport Category Aircraft', Delft University of Technology, Technical Report LR-693, Delft, The Netherlands,1992
35. J. Roskam,'Airplane Design', Roskam Aviation and Engineering Corporation (1986)
36. S. H. Macci,'Semi-analytical Method for Predicting Wing Structural Mass', SAWE Paper No.2282. May 1995
37. Anonymous, MSC Nastran User's Manual. MSC Software Corporation, Santa Ana, California.
38. G. J. Moore,'MSC/NASTRAN - Design Sensitivity and Optimization', The MacNeal-Schwendler Corporation
39. Bruhn, E. F., Analysis And Design Of Flight Vehicles Structures, Jacobs Publishing,1973.
40. E. Torenbeek,'Synthesis of Subsonic Airplane Design', Delft University Press, 1976.
41. Jane,'Jane's, All the World Aircraft', Paul Jackson
42. F.Dorbath, B.Nagel, V.Gollnick,'Comparison of Beam and Shell Theory for Mass Estimation in Preliminary Wing Design', 2nd Aircraft Structural Design Conference, London, 2010